Analyst

TUTORIAL REVIEW

View Article Online
View Journal | View Issue

Cite this: *Analyst*, 2018, **143**, 4819

A pressure-driven gas-diffusion/permeation micropump for self-activated sample transport in an extreme micro-environment

Wenming Wu

The micropump is the most important functional unit of a micro total analysis system (μTAS). An ideal microfluidics system should adopt simple, stable, robust, inexpensive, and integrated on-chip strategies to transport samples for downstream applications, with little or no external energy consumption and limited manual intervention. Nevertheless, it remains a key challenge for traditional micropumps to be directly integrated into self-contained and disposable μTAS for velocity-stable and passive sample transport. The best way to assess the capability of passive micropumps is to evaluate their pumping performance in extreme environments, *e.g.* a 3D configurated microchannel instead of a 2D configuration, high temperature conditions instead of at room temperature, a long microchannel instead of short microchannel, a complex topological microsystem (*e.g.* a microvascular network interconnecting multiple inlets and outlets) instead of a simple topological microsystem (*e.g.* a one-directional microchannel connecting only one inlet and one outlet), and multi-phase microdroplet transport instead of single-phase plug transport. In this review, a novel micropumping methodology – a pressure-driven gas-diffusion/permeation micropump – is described, which is the first review paper dedicated to this subject. A comprehensive overview is provided for comparison between this novel micropumping methodology and traditional passive micropumps, especially for applications in stable velocity control in the aforementioned extreme environments. Compared with mainstream conventional micropumps, we confirm that pressure-driven gas-diffusion/permeation micropumps combine a number of superior properties all into one device, such as small size, simple structure, without the need for microfabrication procedures or external power consumption, strong transport capacity, homogeneous flow velocity, delivery capacity for both multi-phase microdroplets and single-phase plugs, long-distance transport, persistent pumping for both 3D microchannels and complex topological microsystems (*e.g.* a biomimetic microvasculature), low cost, ease of microdevice integration, bubble suppression and amazing stability at high temperatures. An advanced outlook and perspectives for the future development of this novel micropump are also discussed, which may serve as a starting point for researchers in the microfluidics fields to harness pressure-driven gas-diffusion/permeation micropumps for downstream applications.

Received 19th June 2018,
Accepted 6th September 2018

DOI: 10.1039/c8an01120f

rsc.li/analyst

1. Introduction

Micropumps play a crucial role in microfluidic transport and have been a research interest for many years. In the 1980s, Jan Smits and Harald Van Lintel developed the first MEMS micropumps that drive fluid through piezoelectrics.[1,2] During the last 30 years, lots of micropumps have been developed based on different actuation mechanisms. Based on different views, the micropumps can be divided into various subcategories, such as mechanical or nonmechanical micropumps, externally-powered or self-powered micropumps, and on-chip or off-chip micropumps, *etc.* Correspondingly, a series of reviews have been published that cover micropumps from different angles, such as compressive pumping strategies,[3] technological progress and prospects,[4] volumetric power density,[5] flow analysis,[6] BioMEMS platforms[7] and PCR-pump,[8] *etc.*

Different from the aforementioned reviews, herein we mainly focus on addressing the important developments and performance of passive/self-powered micropumps based on the recent literature, and extensively illustrate the pressure driven gas-diffusion/permeation micropump as a novel and promising self-powered on-chip micropumping technique for stable sample transport through a long microchannel. To sys-

State Key Laboratory of Applied Optics, Changchun Institute of Optics, Fine Mechanics and Physics, Chinese Academy of Sciences, Changchun, 130033, China. E-mail: wuwm@ciomp.ac.cn

tematically clarify the differences between this self-powered micropump and traditional pumping types, a brief overview of the mechanisms and performances of traditional external/self-powered micropumps will be outlined first.

External-power driven pumps rely on off-chip power (*e.g.* electricity, mechanics and acoustics) to automate sample flow. Depending on whether mechanical motion is involved or not, they can be separated into mechanical and non-mechanical types. So-called "mechanical micropumps" use the oscillatory or rotational movement of mechanical parts to displace fluids, and can be further divided into different subcategories, such as syringe pumps,[9–13] rotary pumps,[14,15] peristaltic pumps,[16–20] piezoelectric micropumps,[21–23] centrifuge micropumps[24] and (thermo)pneumatic micropumps,[25] *etc.* In contrast, the so-called "nonmechanical micropumps" include electroosmotic micropumps,[26–28] electrokinetic micropumps,[29] magnetohydrodynamic (MHD) micropumps,[30,31] electrochemical micropumps, (electro)magnetic micropumps[32–35] and acoustic micropumps,[36,37] which can transport fluid without any moving components. Although external-power driven micropumps can stably transport liquid, all of them are initiated through the consumption of external off-chip power and are relatively big in size with complex components for liquid displacement, which poses a major challenge for miniaturization and integration into microfluidic devices.

To solve the problem associated with the aforementioned externally-powered micropumps, several types of passive pumping mechanisms that operate *via* surface tension, hydrostatic pressure, gas-solubility/diffusion/permeation, chemical/enzymatic reaction or biophysics, have also been developed to induce fluid flow in microfluidic devices without the need for an external power source. Thus, herein, traditional passive micropumps will be described and then a systemic comparison will be made between pressure driven gas-diffusion/permeation micropumps and traditional passive micropumps.

1.1 Surface tension driven micropumps

The surface tension driven micropump is one typical representative of a self-activated micropump. It utilizes surface tension to spontaneously transport the small volume of fluid that is in contact with the microchannel surface.[38–40] The capillary-pumping method has superiority over external powered micropumps in that it does not require external energy during liquid transport, and thus has attracted increasing interest, especially for use in commercial or clinical applications.[41]

The capillary tension effect can be represented by the following equation:

$$\rho gh = 2\gamma \cos\theta / r$$

where h is the liquid height inside a vertical capillary tube, γ is the surface tension coefficient of the fluid, θ is the contact angle between the fluid and the substrate, ρ is the liquid density, g is gravity, and r is the radius of a capillary tube.

As shown in Fig. 1a, for the three capillary tubes inserted inside the liquid, the liquid heights are different. Because $r_1 < r_2 < r_3$, the liquid heights in the three tubes are $h_3 < h_2 < h_1$, depending upon the above equation.

The above phenomenon explains the mechanism of a capillary pump. The surface tension results in a pressure difference across the liquid–air interface, which is the automation force of a capillary micropump. Through the interplay between the liquid surface tension and the microchannel surface, spon-

Wenming Wu

Prof. Wenming Wu received his BE and BSc dual degrees at the College of Chemistry and Chemical Engineering at the Shandong University in China, and his PhD degree from the Mechatronics department of the University of Saarland in Germany. He is now the hundred talent scholar and doctoral supervisor at the Chinese Academy of Sciences, as well as the group leader of the State Key Lab of Applied Optics (SKLAO) and the Changchun Institute of Optics, Fine Mechanics and Physics (CIOMP). His research interests lie in the development of miniaturized devices mainly focusing on leaf-inspired biomimetics, multiplex and real-time PCR, cell-/tissue-/organ-on-chip research, and the integrated functionalization of microTAS systems. Over the past five years, Prof. Wenming Wu has invented more than 10 new micro-manufacture technologies, spanning over 20 first/corresponding authored SCI papers and patents.

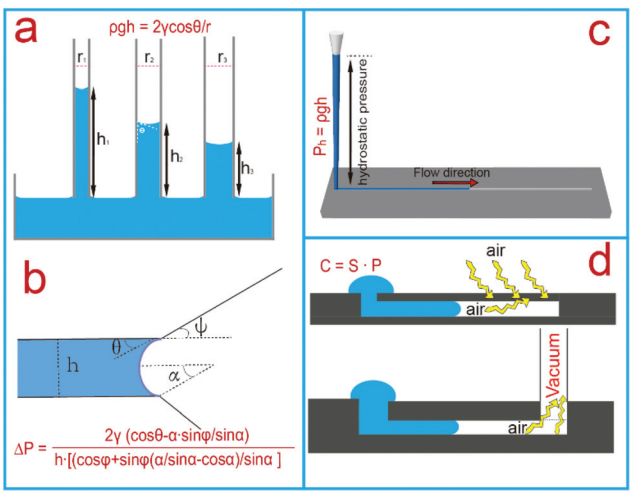

Fig. 1 Traditional self-powered micropumps. (a) Schematic diagram of the capillary tension effect. (b) Illustration of hydrophobic barriers (capillary valving elements) resulting from a geometric change in the microchannel. The fluidic front within the microchannel is denoted by the blue arc. (c) Schematic diagram of the hydrostatic pump. (d) Schematic diagram of a vacuum driven gas-diffusion/permeation micropump.

taneous flow is maintained in the direction that minimizes the free energies between the fluid and solid interface. The capillary pressure P_c can be calculated using the following equation:

$$P_c = 2\gamma \cos\theta / r$$

where P_c is the capillary pressure.

Depending on this equation, we can see that the capillary pressure increases as the channel surface tension increases. In most cases, the microchannel is a rectangular cross section. Correspondingly, the aforementioned equation can be modified to:

$$P_c = 2\gamma \cos\theta (W + H)/WH$$

where W and H are the width and height of the microchannel, respectively.[42]

According to the aforementioned equations, only contact angles of less than 90° can produce a positive pressure (P_c) onto the sample, to motivate it flow forward through the microchannel, otherwise the liquid will stop. Because of this, naturally hydrophilic substrates, such as glass,[43,44] silicon,[45–47] metal, some types of polymer (*i.e.* poly(methyl methacrylate) (PMMA)[42] and polyester polyethylene terephthalate (PET)),[48] Norland optical adhesive (NOA) substrates, hydrogels[49] and paper (wicking flow),[50] are ideal materials for application in capillary pumps. Although it is more difficult for hydrophobic materials (*e.g.* polydimethylsiloxane (PDMS)[51] and polycarbonate (PC)[52]) to be applied in capillary pumps compared to hydrophilic materials, proper surface modification such as plasma treatment,[53] UV–ozone treatment, reagent spotting or vapor deposition[54] and chemical adhesion (hydrophilic reagents into the channels)[50–52] can easily change the hydrophobic/hydrophilic properties of the channel surface. Besides this, the contact angle of the hydrophilic surface can also be changed through surface modification, to further adjust the pumping pressure. In some extreme cases, a super-hydrophobic surface can also be applied for surface tension motivated flow. For instance, it has recently been reported that a superhydrophobic plate filled with water can be presented for sustained long distance liquid transport to over 100 mm in height with an average transport speed of 4500 mL h^{-1}.[55]

Depending on the aforementioned equation, capillary flows are virtually determined by three main factors, the surface tension γ, the liquid contact angle θ, and the geometrical characteristics (r, W or H) of the flow channel/domain. For example, it has been discovered that the channel height,[53] channel width and sector-shaped paper with different angles, or the angle of fan-shaped filter paper,[56,57] can modulate the flow rate for self-powered programmable control inside microdevices. The function of a surface tension-driven micropump can be expanded through the integration of hydrophobic barriers (capillary valving elements) into a microdevice through changing the structural geometry, surface tension or contact angle control of the micro-scaled surface. Assuming that the width of the microchannel is much larger than its height,[58] hydrophobic barriers can be represented by the following equation:

$$\Delta P = \frac{2\gamma}{h}\left[\frac{\cos\theta - \frac{\alpha}{\sin\alpha}\sin\varphi}{\cos\varphi + \left(\frac{\alpha}{\sin\alpha} - \cos\alpha\right)\frac{\sin\varphi}{\sin\alpha}}\right]$$

where θ is the contact angle, h is the channel depth, γ is the surface tension coefficient, ΔP is the pressure barrier, α is the curvature of the meniscus, and φ is the change in angle for the new direction of fluidic flow, as shown in Fig. 1b.

So, a sudden change in channel cross section, surface tension or contact angle can vary the capillary pressure, which further accelerates, slows down or even stops the liquid flow. Depending on the valving element, a microfluidic conduit can be designed in an electronic-circuit form with integrated functions.[51]

1.2 Hydrostatic-pressure driven micropumps

In most cases, surface tension driven micropumps require a hydrophilic surface to induce spontaneous flow, which limits their application areas. In contrast, hydrostatic pumps are compatible with either hydrophilic or hydrophobic surfaces that make up the microchannel. In such type of micropump, a vertical tube is connected to the microchannel, which can produce hydrostatic pressure on the liquid.[59,60] As long as the device is on the ground, a hydrostatic pressure can be maintained to automate the liquid flow, requiring no other power source.[61]

Hydrostatic pressure can be represented by the following equation:

$$P_h = \rho g h$$

where P_h is the hydrostatic pressure, ρ is the liquid density, g is gravity, and h is the liquid height inside the vertical tube.

As shown in Fig. 1c, the hydrostatic pressure on the microchannel can be controlled by intensity and height of the liquid connected to the inlet. In addition to gravity, buoyancy is another form of hydrostatic pressure, which has been also applied for liquid flow. Depending on Rayleigh–Bénard convection and the buoyancy effect, a portable polymerase chain reaction system (PCR) was realized inside a single tube, which can successfully amplify phage DNA within 15 min.[62] Both surface tension-driven micropumps and hydrostatic micropumps have little interference on the properties of the sample transported.

1.3 Vacuum-driven gas-diffusion/permeation micropumps

Over a decade ago, a practical and self-powered autonomous pump was proposed for liquid transport inside PDMS channels without the need to functionalize the channel surfaces from hydrophobic to hydrophilic. For instance, just by putting PDMS inside a vacuum chamber for an amount of adequate time,[63,64] self-powered autonomous flow can be realized inside portable PDMS microfluidic devices. For this pumping technology, air permeability of the microdevice is the key determinant in realizing self-powered pumping. However, depending

on the detailed mechanism, this pumping can be further classified into several subtypes depending on whether the microchannel itself or an external accessory functions as a suction source.

If the microchannel itself can automatically suck the sample inside, such a microdevice can be designed to be more portable and compact, because it doesn't require any extra on/off-chip microfluidic units. During the sample injection, air molecules encapsulated inside the microchannel can diffuse through the diffusive and permeable wall of the PDMS microchannel, resulting in relatively lower pressure at the anterior rather than the posterior end of the sample, thus forming a suction force that automates the sample to flow toward the outlet. The high gas solubility of elastomeric PDMS has been exploited to provide various low-cost, user-friendly, power-free, and self-contained microsystems for autonomous sample injection for use in downstream applications.[65–68] For instance, after preevacuation of the whole PDMS substrate, the sample and oil can be sequentially sucked into the microarray to self-compartmentalize the sample *via* 5120 independent microchambers, each 5 nL in volume.[69] Similarly, after being degassed in a vacuum chamber, a self-priming PDMS spotter containing regular micro-holes and embedded microchannels has been applied to autonomously produce uniform microarrays with a measured coefficient of variation (CV) for 48 spots of 2.63%.[70] An air-evacuated PDMS channel that is capable of generating monodispersed droplets with a coefficient of variation below 3% has also been previously reported.[71]

The aforementioned degassed PDMS pumps were generally restricted to PDMS microfluidic devices, which are gas permeable. To realize vacuum driven self-powered flow inside microchips that are not gas-diffusive/permeable, some other air-evacuated pump modules have also been introduced. One method operates through desorption of a PDMS slab and an integrated mesh-shaped chamber. After placing the degassed PDMS slab on the outlet of microfluidic devices (either gas-permeable or gas-impermeable), the PDMS slab can absorb the air in the microfluidic system,[94] offering various pumping capacity by varying the geometries of the slab module.[72] However, the mechanism of this method is still similar to that of the previous case in that it relies upon the preevacuation of the whole PDMS substrate, and has been systematically studied in previous research.

Briefly, because PDMS is gas soluble, it can absorb gas, as characterized by solution and diffusion processes. The gas solubility is linearly pressure-dependent in PDMS, and can be described in terms of Henry's law as follows:

$$C = S \cdot P$$

where C is the concentration of gas molecules in PDMS, S is the solubility coefficient of gas in PDMS, and P is the gas pressure.

It can be easily seen that at lower pressure, the number of air molecules encapsulated inside PDMS is proportionate to the volume of the PDMS slab, and decreases with a drop in the vacuum level during the degassing step. As a result, after the degassed PDMS is placed back under atmospheric pressure, the air molecules around the PDMS diffuse into the interior of the PDMS to create a negative pressure, thus driving the sample to automatically flow from the inlet to the outlet of the microchannel.

Despite its simplicity of pumping control, there are several disadvantages associated with these vacuum-driven self-powered micropumps. Firstly, the PDMS devices or slabs need to be stored in an airtight package, because they will lose pumping power within a short time under atmospheric pressure. Secondly, the PDMS devices or slabs need to be prevacuumed for a sufficient time (tens of minutes to 24 hours)[68] depending on the geometric parameters before use, and thus, they are impossible to use for instantaneous pumping processes. Thirdly, generally they can only automate unidirectional transport, making them impossible to use once the microchannel is filled with liquid. Fourthly, a stable flow rate is difficult to achieve by vacuum-driven pumping methodology.

To solve these issues, a syringe-assisted vacuum-driven micropump[73] was also introduced, which not only enables instantaneous pumping, but also allows bidirectional flow through the microchannel, as previously reported.[74] This was realized through a pneumatic chamber connected to the microchannel by a gas permeable PDMS membrane[75] or PDMS wall.[76] Through the control of the pressure inside the pneumatic chamber, the gas molecules can be controlled to either pass through the PDMS membrane/wall from the microchannel to the chamber (vacuum mode), or the opposite (pressure mode). Air flux through a thin membrane/wall permits an instant steady-state pumping performance. One advantage of this method is that it can produce much more stable pumping velocity than degassed PDMS devices. As previously reported, a stable flow rate can be realized during the majority of the flow period through a 1.4 cm microchannel when its outlet is vacuumed by a hand-held syringe. On the other hand, issues associated with labour, time and cost of microfabrication increase for this method since the PDMS wall or PDMS membrane should be integrated into the devices, which in turn also decreases the density of the functionalized components of the microfluidic chip, because the PDMS membrane/wall and pneumatic microchambers occupy chip-space.

Besides this, a tiny microchannel can also be used to replace the PDMS membrane/wall to automate self-powered liquid transport,[77] using a vacuum produced by a hand-operated syringe connected to the outlet of a flow-through microchannel. After connecting a 10 ml Becton Dickinson plastic syringe to the outlet of a PDMS device through a 16 G needle and PE/5 tubing, mono-dispersed emulsions can automatically form, with a droplet size and production frequency controlled by channel resistance. Finally, the droplets flow out of the device into the vacuum syringe, and can be collected, stored and incubated in the syringe for further assay.

1.4 Self-powered chemical/biological micropumps

Other types of self-powered micropumps have also been developed, which are driven by chemically[78–82] or biologically[83] auto-

mated mechanisms. Although some of these chemical and biological pumps can be classed as self-powered transport types, herein we will not systematically review these pumps because their capability for accurate and stable flow control still requires further investigation in contrast to the aforementioned main stream self-powered pumping methods. For more information, see a related review in the literature for reference.[84]

2. Pressure-driven gas-diffusion/permeation micropumps

In earlier studies, pressure-driven gas-diffusion/permeation micropumps were only used for simple microfluidic transport. For instance, bidirectional flow was reported after the liquid was firstly sucked from the channel inlet into a dead-end by a vacuum mode, and then a pressure mode was used to realize pressure-driven backflow through a permeable PDMS membrane.[74] The bubble-free sample injection into a PDMS device with a simple architectural geometry has also been realized using a pressure-driven mode.[85] However, the study of accurate flow control and velocity programming by gas-diffusion/permeation micropump was rarely clarified before 2012.

Depending on the improvements in injection approaches, as demonstrated in recent reports after 2012,[86–90] the aforementioned challenges associated with pressure-driven permeation/diffusion micropumps have been well solved, using instruments as simple as vacuum driven diffusion/permeation micropumps. However, there is big difference in the operational procedure compared with that of a depressurization air-driven micropump. Fig. 2 shows a schematic illustration revealing the actuation mechanisms of two types of pressure-driven gas-diffusion/permeation micropumps. Briefly, the air pressure throughout the entire microfluidic conduit is the same as before introducing the sample plug into the microdevice. After the introduction of the sample into the inlet tube of the microchip, the sample plug separates the fluidic conduit into two parts, wherein larger amounts of air-molecules permeate through the anterior part of the sample plug *via* the gas-permeable surface of the fluidic conduit than the posterior part of the sample plug, which is a gas-impermeable plastic syringe. And thus, this causes a relatively higher internal pressure in the posterior end than in the anterior part of the sample plug, automating the movement of the sample.

As shown in Fig. 2, only a few tools are required to activate sample flow in a pressure-driven permeation/diffusion micropump, proving that the use of a pressure-driven diffusion/permeation micropump is as simple as a self-powered vacuum-driven diffusion/permeation micropump. After injection, the sample can spontaneously flow to the end of the microchannel. If two inlets are connected to the fluidic conduit, the delivery of double-phased microdroplets can be automated (Fig. 2a). It is notable that the volume ratio of the oil-phased syringe to the ink-phased syringe (V_1/V_2) determines the volume ratio of the oil droplets to sample droplets (V_{oil}/V_{sample}) and the flux ratio (U_{oil}/U_{sample}). If only one inlet is connected

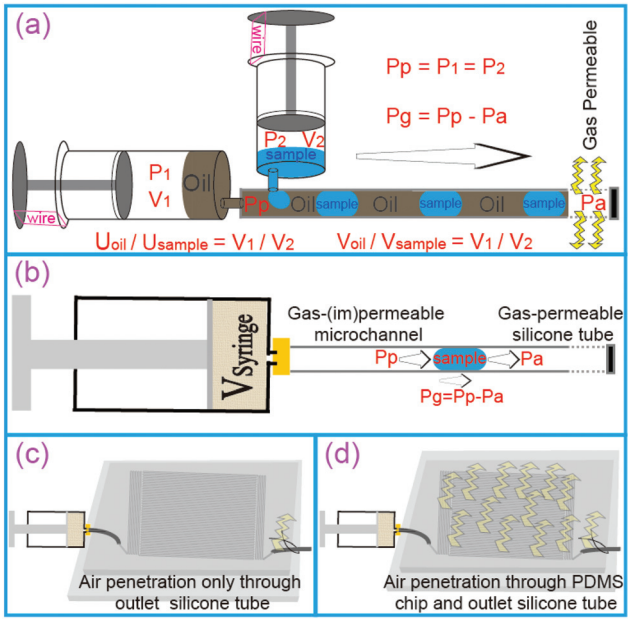

Fig. 2 A schematic illustration demonstrating the pressure-driven gas-diffusion/permeation micropump as a new self-activated micropump for sample transport with high homogeneity. (a) The microdroplet delivery. (b) The plug delivery. (c) The mechanism of the pressure-driven gas-diffusion/permeation micropump, based on air permeability through the outlet tube. (d) The motivation mechanism for the pressure-driven gas-diffusion/permeation micropump, caused by air diffusion/permeability to the atmosphere through the inlet tube, permeable microdevice and outlet tube.

to the fluidic conduit, the delivery of a single-phased plug can be automated (Fig. 2a).

Altogether, two automation mechanisms have been discovered. Both of them are based on the air permeability from the fluidic conduit to the atmosphere, since the pressure of the compressed air captured inside the closed fluidic conduit is higher than the atmospheric pressure. If the microchip is fabricated from a gas impermeable material (Fig. 2c) such as PTFE[91] and PMMA,[89] a pressure-driven gas-diffusion/permeation micropump can be realized just by connecting a piece plug of silicone tube (gas-permeable) to the microchip, which can automate a stable flow rate.

If the microchip is fabricated from a gas permeable material (Fig. 2d), such as PDMS[86,90] and silicone tubing,[88] then a pressure-driven gas-diffusion/permeation micropump can be realized based on the same operational procedure, but the flow rate will dramatically decrease as time goes on. So, the flow characteristics resulting from these two different automation mechanisms are totally different, and have been studied in detail in our previous works.

3. Velocity assays of self-powered micropumps

To precisely and stably modulate the flow rate inside the microchannel is one foundational function of all micropumps.

However, despite the dramatic achievements in the development of different pumping mechanisms for fluidic transport over the last few years, it has become the main bottleneck[92] in realizing a passive micropump that can provide a homogeneous and stable flow rate for applications in extreme microenvironments. Thus, the approaches in stabilizing the flow rate using self-powered micropumps will be discussed in the next section.

3.1 Surface tension micropumps

Generally speaking, the flow rate which is automated by passive micropumps tends to slow down as time passes, due to time-lapsed decreased pumping power or increased flow resistance.

Based on the Hagen–Poiseuille equation, the flow resistance can be calculated using the following equation:

$$P_r = 8\mu l \frac{u_l}{r^2}$$

where P_r is the resistance pressure, l is the length of the liquid plug inside the microchannel, u_l is the flow rate of the liquid if the flow distance is l, μ is the liquid viscosity, and r is the channel radius.

As can be easily seen, as more and more fluid flows into the microchannel, l increases and thus, the resistance pressure P_r increases if there is no change in the flow rate. However, for surface tension micropumps, the pumping power P_c remains constant, assuming that there is no change in structural geometry, surface tension and contact angle control of the microchannel.

In static flow, it can be considered that $P_c = P_r$. So, P_r is assumed as a constant amount.

Because $u_l = \frac{dl}{dt}$, then $8\mu l \frac{dl}{r^2 dt} = P_c$ can be derived, and then, because

$$l^2 = \frac{r^2 P_c}{4\mu} t,$$

a new equation can be derived:

$$l = \left(\frac{r\gamma \cos\theta}{2\mu}\right)^{\frac{1}{2}} \sqrt{t}$$

The above equation indicates that for the surface-driven flow, the flow distance is linearly proportional to the square root of time. As a result, homogeneous velocity cannot be realized in classic surface tension-driven flow, but instead, the velocity decreases as the time lapses, assuming no change in structural geometry, surface tension and contact angle control of the microchannel.

Systematic studies on surface-driven wicking flows have been done inside a 50 mm channel.[93] It was observed that for different types of paper substrates, different flowing-out times were required as follows: 18 min (Roth 15A), 16 min 30 s (lab-engineered cotton linter-based paper, 76 g m^{-2}), 8 min 30 s (Whatman no. 1), and 6 min 10 s (lab-engineered eucalyptus sulfate-based paper, 95 g m^{-2}). Despite the wide range of flow rates inside the different substrates, the flow rates inside all the paper-defined channels exactly obey the expected $l = \propto\sqrt{t}$ rule, as shown in Fig. 3A.

To solve the aforementioned non-stable automation problems associated with surface tension-driven micropumps, the fluid dynamic model was also derived and calculated, to validate an accurate flow rate by changing the geometrical shape

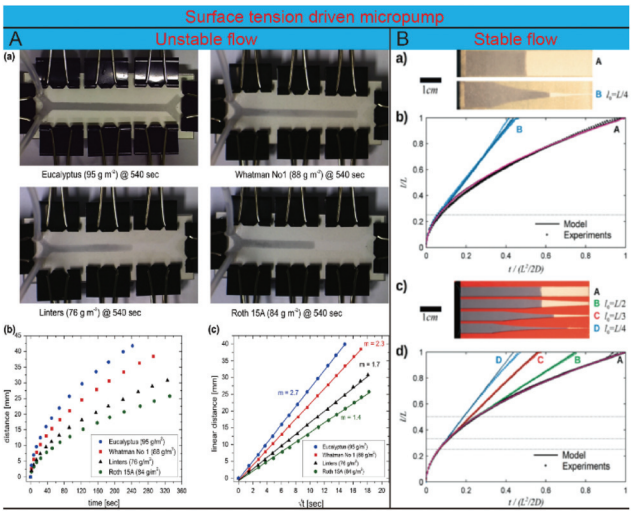

Fig. 3 (A-a) Comparison of the fluid front inside the paper-defined channels for different paper substrates at a given time interval. Photographs were taken 9 min after the fluid was brought into contact with the channels. (A-b) Comparison of the fluid front driven by capillary action along the channel as a function of time for the investigated paper substrates. Individual data points were captured by video streaming the capillary transport of the fluid inside the channel. The expected relationship between the distance and time was observed for all paper substrates; that is, the further the distance of the fluid front from the channel inlet, the longer the time taken by the fluid front to move a certain distance inside the channel. By using different paper sources, the distance covered by the fluid front within a given time interval was controlled over a wide range. (A-c) Comparison of the fluid front driven by capillary action along the channel as a function of $t^{0.5}$ for the investigated paper substrates. Reproduced from ref. 93 with permission from Springer Nature, copyright 2014. (B) Experimental results of fluid imbibition in both paper strips and slit microchannels. (B-a) Photograph of the paper-based microfluidic device during imbibition. The image was taken at $t \sim 225$ s after water imbibition began. The dark blue areas are wetted zones. The strips labelled A have a constant width and were used as a reference. The strips labelled B have exponentially varying widths to produce constant fluid velocity at the advancing front. (B-b) Experimental data (symbols) and model predictions (lines) of the liquid front position as a function of non-dimensional time for the strips shown in (B-a). The horizontal dotted line indicates the position at which the exponential section begins. (B-c) Photograph of the slit microchannels during imbibition. The image was taken at $t \sim 35$ s after liquid imbibition began. The dark blue areas are filled zones. The slit labelled A has a constant width. The slits labelled B, C, and D had exponentially varying widths, with initial loads of length $L/2$, $L/3$, and $L/4$, respectively. (B-d) Experimental data (symbols) and model predictions (lines) of the liquid front position as a function of non-dimensional time for the slit microchannels shown in (B-c). The horizontal dotted lines indicate the positions at which the exponential section begins. Reproduced from ref. 94 with permission from the Royal Society of Chemistry, copyright 2015.

(cross section) of the substrate.[94] Although the surface tension-driven flow rate can be controlled to be homogeneous through this approach, both theoretical investigations and complicated geometric designs are required.

3.2 Hydrostatic pressure-driven micropumps

Similar to surface tension-driven micropumps, the flow velocity automated by a typical hydrostatic pump also decreases as the time lapses. In a hydrostatic pump, a vertical column/tube containing liquid is connected to the microchip to realize hydrostatic pressure. Because fluidic surface tension is nonnegligible at the micro-level, the overall/calibrated pumping pressure should be a combination of both the hydrostatic pressure and capillary force, which can be represented by:

$$P_o = P_g + P_c = \rho g h - 2\gamma_m \frac{\cos\theta_m}{r_m} + 2\gamma_v \frac{\cos\theta_v}{r_v}$$

where P_o is the overall pressure, ρ is the liquid density, g is gravity, h is the hydrostatic height inside a vertical tube/column, γ_v, θ_v, and r_v are the surface tension, the contact angle and the radius at the posterior end of the fluid plug, and γ_m, θ_m, and r_m are the surface tension, the contact angle and the radius at the anterior end of the fluid plug.

For stable flow,

$$P_o = P_r = 8\mu l \frac{u_l}{r^2}$$

As more and more fluid flows into the microchip from the inlet to the outlet, the hydrostatic height between the inlet and outlet reservoirs drops, further decreasing the hydrostatic pressure. As a result, the hydrostatic-driven flow rate decreases correspondingly, which limits the application of the hydrostatic pump in downstream applications. In a previous report, such dramatic increase of flow rates was confirmed by varying the hydrostatic heights and the widths of microchannel as 50, 100, 250, and 500 μm, respectively.[95]

A stable flow rate by hydrostatic micropump is determined by three key factors: the hydrostatic pressure P_g, the flow resistance P_r, which is mainly determined by the length of the fluidic plug inside the microchannel l, and the surface tension at the posterior/anterior end of the fluid plug. However, if the hydrostatic pressure is much larger than the surface tension pressure (*e.g.* the hydrostatic height is high, or the contact angle is close to 90 degrees), then the overall pressure is mainly determined by the hydrostatic pressure.

Until now, various techniques have been developed to realize sample transport at constant velocity by hydrostatic pump. One approach is through the connection of a horizontal reservoir[96] to the vertical column/tube. As long as there is a liquid plug inside the horizontal reservoir during the fluidic flow, then Δh can be kept constant to realize stable hydrostatic pressure P_g (Fig. 4A). In addition, surface tension at the posterior and anterior end of the fluid plug can be made constant if there is no change in the reservoir geometry and materials. Since the microchannel of the microdevice is totally filled with liquid during sample transport, there is no change in the total length of the liquid plug inside the microchannel. As a result, the above equation can be satisfied at a constant flow rate because the flow resistance P_r can be maintained to be the same as the overall pressure P_o.

3.3 Vacuum-driven gas-diffusion/permeation micropumps

Vacuum-driven gas-diffusion/permeation micropumps take advantage of the inherent solubility of gas, diffusion and permeation of PDMS elastomer to initiate flow. For degas-driven diffusion micropumps, the effect of various parameters on the dynamics of degas-driven flow have been systematically studied, including the channel geometry, the PDMS thickness, the PDMS exposure area, the vacuum degassing time, and the idle time at atmospheric pressure before loading.[68] A reproducible flow with a standard deviation of less than 8% for a flow velocity ranging from approximately 0.2 to 3 nL s^{-1} has been achieved inside microchannels that are 25 to 65 mm in length. However, unfortunately, none of these parameters[68] can produce a stable flow rate, highlighting the difficulty of using a vacuum-driven gas-diffusion micropump to realize a stable flow. In contrast, better flow control can be achieved by utilizing vacuum-driven gas permeability of a PDMS wall/mem-

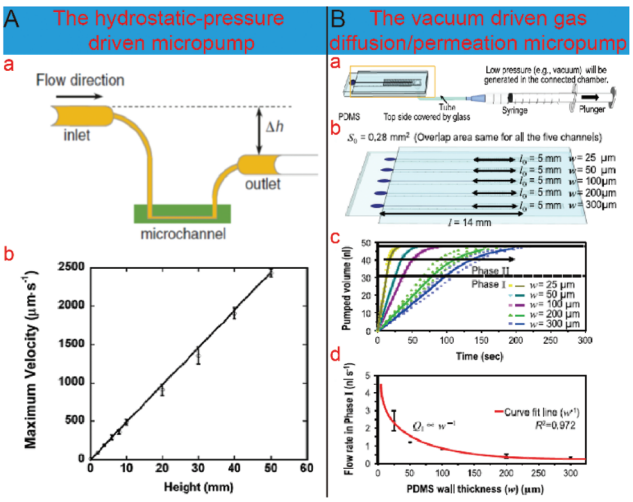

Fig. 4 (A) Effect of the height differences on the flow velocity. (A-a) A schematic illustration of the one-inlet–one-outlet of the gravity-driven pump with horizontally oriented fluid reservoirs. (A-b) The flow velocity increases linearly as the height difference increases. The pumping velocities of water were determined at various operating heights. The experimentally measured velocities are compared with the expected velocities from theoretical calculations (solid line). The error bars show the standard deviation. Reproduced from ref. 96 with permission from the Royal Society of Chemistry, copyright 2004. (B-a) Schematic illustration of the proposed syringe-assisted vacuum-driven gas-diffusion/permeation micropump. (B-b) Effect of the overlap area between the channel and embedded microchamber on the syringe-assisted vacuum-driven gas-diffusion/permeation micropump. Schematic diagram showing devices with varying overlap areas (*e.g.* 0.00345, 0.176, 0.521, 0.693, and 0.866 mm^2), while the thickness of the PDMS wall is maintained at the same value (w = 50 μm). (B-c, B-d) Pumped volume profiles *versus* time with different overlap areas. Reproduced from ref. 73 with permission from Springer Nature, copyright 2014.

brane.[73] Through controlling the overall area (between the microchannel and embedded vacuum microchamber) or the thickness of the PDMS wall/membrane, the self-powered flow rate can be adjusted from 0.089 to 4 nl s^{-1}. Although a good linear relationship between the pumped volume and time can be achieved in the earlier stage of sample flow through a 35 mm long microchannel, the flow rate is dramatically slowed down especially when it is close to the end of the microchannel (Fig. 4B).

3.4 Pressure-driven gas-diffusion/permeation micropumps

In contrast with the aforementioned types of micropump, pressure-driven gas-diffusion/permeation micropumps can be applied for sample transport under more extreme microconditions: such as long microchannels (several meters) and high temperature. Depending on the gas permeability of the fluidic conduit, pressure-driven gas-diffusion/permeation micropumps can be classified into two subcategories, as shown in Fig. 2. There are obvious differences in the flow characteristics of each subcategory.

3.4.1 Unstable, slow gas-permeable microdevices. If pressure-driven gas-diffusion/permeation micropumps are applied to gas-permeable microdevices, then the pumping power decreases rapidly as the sample flows through the microchannel. Fig. 5A shows the experimental results of a pressure-driven gas-diffusion/permeation micropump for self-powered sample transport inside a gas-permeable fluidic conduit: a silicon tube (i.d. 0.5 mm, o.d. 2 mm). Fig. 5(A-a) and (A-b) show the effect of the tube length on the total running time of the ink solution and flow rate variation pattern at certain lapse times, respectively, when the initial internal pressures of the tubes were fixed at 1.61 atm (by pushing the piston from 4.6 to 2.8 mL of the syringe graduation). Fig. 5(A-c) and (A-d) show the effects of the initial internal pressure of the tube on the total running time of the ink solution and flow rate variation pattern at a certain lapse time, respectively, when the total lengths of the tubes were fixed to 95 cm. Although in these experiments, the effects of the total length and initial internal pressure of the tube were mainly investigated, all of the results showed an obvious time-lapsed drop in the flow rate.

Self-powered flow of multi-directional microchannels inside a PDMS microchip has also been characterized and analyzed using three types of biomimetic microvascular networks (fabricated from different leaves: Tilia platyphyllos, Aegopodium podagraia and Carpinus betulus). Despite the obvious geometric difference in the single-directional silicone tubing device, the flow velocity showed similar flow properties, which dramatically slowed down as the time passed. Surprisingly, it was found that the flow rate of a leaf-inspired microdevice obeyed the sorptivity rule, which is mostly related to the aforementioned capillary absorption. As shown in Fig. 5C, the flowing distance (amount) in both the 1st microchannel and the 2nd ordered microchannels of the PDMS leaf from Carpinus betulus, were linearly correlative with the square root of time, obeying the sorptivity rule.

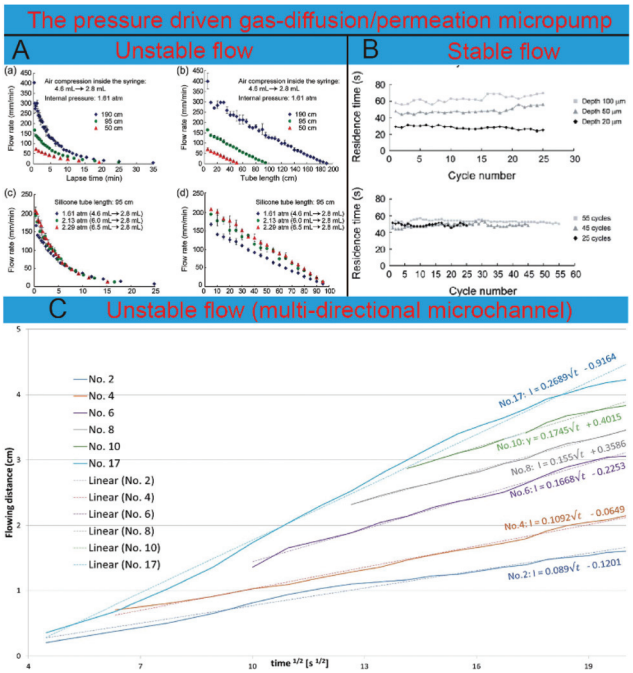

Fig. 5 (A) Quantitative analyses of the proposed sample injection scheme employing silicone tubes (i.d. 0.5 mm, o.d. 2 mm). (A-a)–(A-b) The effect of the total tube length on the total running time and flow rate variation pattern when the internal pressure was fixed at 1.61 atm. (A-c)–(A-d) The effect of the initial internal pressure on the total running time and flow rate variation pattern, when the tube lengths was fixed at 95 cm. Reproduced from ref. 86 with permission from the Royal Society of Chemistry, copyright 2012. (B) Effects of depth of the PMMA microchannel, and total length of the PMMA microchannel (1.25, 2.25 and 2.75 m corresponding to cycle numbers 25, 45 and 55) on the speed and uniformity of the sample flow. Reproduced from ref. 89 with permission from the Royal Society of Chemistry, copyright 2015. (C) Quantitative flow analogy inside a PDMS leaf containing parallel networks replicated from Carpinus betulus, with the flowing distance plotted *versus* the square root of time. Reproduced from ref. 87 with permission from the Royal Society of Chemistry, copyright 2016.

During sample flow, the air permeates through both the posterior end and the anterior end of the sample plug of the microdevice. As the sample plug flows from the inlet toward the outlet through the microchannel, the diffusion area at the posterior end tends to increase. Meanwhile, the diffusion area at the anterior end tends to decrease. As a result, the pressure gradient imposed on the sample plug, which is virtually caused by the inhomogeneous diffusion extent between the anterior and posterior ends of the sample plug, tends to decrease, and further induces a gradual reduction of the pressure gradient (Fig. 5A and C) and also a drop in the velocity. So, the sample velocity becomes slower and slower as the sample flows forward.

3.4.2 Stable flow gas-impermeable microdevices. If pressure-driven gas-diffusion/permeation micropumps are applied in gas-impermeable microdevices, the flow stability can be greatly improved than for all the aforementioned self-powered micropumps. Gas permeation can be initiated by

connecting a silicone tube to the outlet of the fluidic conduit and being blunt-ended by a commercial clamp. As has been systematically studied in 2D PMMA and 3D PTFE microchips containing microchannels of several meters in length, it was found that the pumping power of the pressure-driven gas-diffusion/permeation micropump can be stably maintained as the sample flows through the microchannel. Fig. 5B shows the experimental results of a pressure-driven gas-diffusion/permeation micropump for self-powered sample transport inside a gas-impermeable microchip. Evaluation of the self-actuated liquid flow is presented through varying the length of the outlet silicone tube, the cross section of the microchannel, and the total length of the microchannel. It was found that the flow rate can be obviously influenced by both the channel depth and tube length, as shown in Fig. 5B. In contrast, the total length of the microchannel does not influence the flow rate, but changes the overall flow-out time.

The relationship between the flow rate, the operational parameters and device dimensions can be represented by the following equation:

$$Q_a = G_a = \frac{2\pi LD}{RT \ln\frac{r_o}{r_i}}(P_a - P_{atm}) = \vartheta H_c W_c$$

where Q_a is the fluidic flux, G_a is the diffusion flux, ϑ is the velocity of the microfluidics, H_c is the height of the microchannel, W_c is the width of the microchannel, D is the effective diffusion coefficient, P_a represents the air pressure in the anterior end of the sample plug, P_{atm} is the atmospheric pressure, P_g represents the pressure gradient imposed in the sample plug, r_i and r_o are the inner radius and outer radius of the outlet tube, T is the temperature in Kelvin, and R is a gas constant. So, the velocity of a stable flow can be adjusted by the tube permeability (D), length (L), tube inner diameter (r_i), inner compressed pressure (P_a), tube outer diameter (r_o), and the width W_c and height H_c of the microchannel.

For this type of gas-permeable microchip, the air permeates only through the outlet silicone tube that is located at the anterior end of the sample plug. Because the inlet tube, the gas-impermeable chip, and the disposable syringe have much weaker gas-permeable properties than those of the outlet silicone tube, it can be reckoned that air molecules only permeate from inside the fluidic conduit to the ambient atmosphere through the outlet silicone tube, and thus, the gas permeability at the posterior end of the sample is negligible. For easier modeling of such a self-activated pumping system, an equilibrium state forms during the same transport when the flow-flux (liquid) and penetration-flux (gas) reach the same value. Under such an equilibrium state, the pressure at the anterior end of the sample plug remains consistent, which causes a constant pressure gradient to be imposed in the sample plug, and thus, stabilizes the homogeneity of the flow rate for both 2D and 3D microchannel configurations.

3.5 Comparison between pressure and vacuum gas-diffusion/permeation micropumps

The mechanism of self-powered pressure-driven gas-diffusion/permeation micropumps, to a certain extent, is similar to that of a vacuum-driven gas-diffusion/permeation micropump, because both systems rely on air-permeable materials to realize self-powered autonomous flow. As aforementioned, the gas solubility/permeability of PDMS is a precondition of self-powered vacuum-driven gas-diffusion/permeation micropumps. If the microdevice is air impermeable, then self-powered autonomous flow cannot be realized in both vacuum-type and pressure-type systems.

The diffusion and permeation process of air from inside the microdevice to the ambient environment automates the liquid flow. As a result, if the microdevice is placed inside a water bath, more air bubbles can be seen on the device surface as the time passes, as shown in Fig. 6. Because inhomogeneous gas transport between the anterior and posterior part of the sample activates the pumping effect, bubbles can be visualized on the surface of the microdevice inside the water bath.

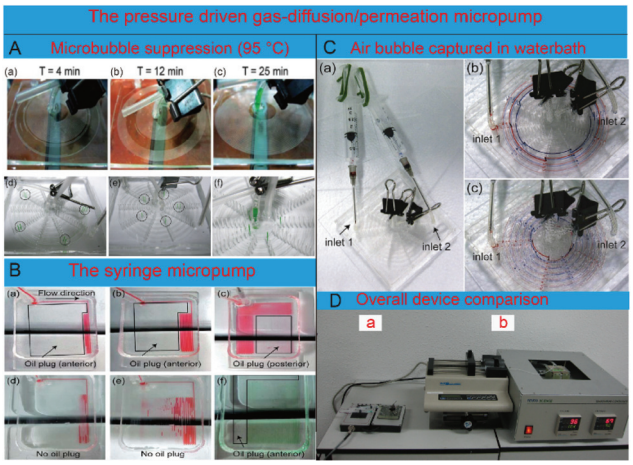

Fig. 6 (A-a)–(A-c) A series of photos demonstrating the suppression of air bubbles with the flow of the PCR sample inside a spiral microchannel in a time dependent manner under heated conditions, measured at 4, 12, and 25 min. Reproduced from ref. 86 with permission from the Royal Society of Chemistry, copyright 2012. (A-d)–(A-f) Time-dependent sample flow inside a two-layer microdevice actuated by a pressure-driven gas-diffusion/permeation micropump, demonstrated under heated conditions employing a green-colored PCR mixture. (B-a)–(B-c) Bubble elimination when paraffin oil plugs are employed both in the anterior and posterior part of the ink plug. (B-d)–(B-e) Bubble generation when paraffin oil plugs are not employed. (B-f) Bubble elimination when a real sample was encapsulated within paraffin oil plugs both in the anterior and posterior of the sample. A green-colored buffer was utilized for visual effect. Reproduced from ref. 10 with permission from the Royal Society of Chemistry, copyright 2011. (C) Air bubble captured on the surface of the microdevice. Reproduced from ref. 90 with permission from Elsevier Science & Technology Journals, copyright 2013. (D) Overall systems needed to operate PDMS microdevices based on (D-a) a self-powered pressure-driven gas-diffusion/permeation micropump and (D-b) a syringe pump. Taken from (Wu *et al.*, Sens. Actuators, B, 2013, **181**, 756) with modification.

It is easy to understand how a vacuum-driven diffusion/permeation pump can automate sample transport, either concerning its diffusion mechanism or permeation mechanism. However, there are some obvious challenges in utilizing pressure-driven diffusion/permeation micropumps for accurate flow control, and thus they can only be applied for the simple format of long term transport.[74,85] For diffusion-type self-powered pressure-driven gas-diffusion/permeation micropumps, it is difficult for the sample to be automatically sucked into a PDMS microchannel, assuming it has been placed under a high pressure for sufficient time (but this is easily realized by the vacuum-type), because the amount of air molecules dissolved in PDMS dramatically increases under a pressurized environment than under atmosphere conditions. As a result, after the pressurized PDMS channel is placed back into the atmosphere, gas molecules diffuse from the pressurized PDMS slab into the channel, and thus cause a higher pressure inside the microchannel than its inlet, which in return prohibits the sample from being sucked in. The situation is similar for the permeation type, because for a channel pressure higher than atmospheric pressure, it seems impossible to suck the liquid plug into the pressurized microchannel from the inlet, let alone there being the capacity to drive the liquid flow through the long microchannel (*i.e.* several meters) towards the outlet.

So, how to solve the aforementioned problems associated with pressure-driven permeation/diffusion micropumps, has been a challenge for many years. And thus, new techniques should be introduced to automate pressurized air-driven micropumps for sample transport. In previous works,[86–90] a series of new methodologies were introduced for accurate flow control by self-powered pressure-driven gas-diffusion/permeation micropumps, without any fabricating steps or any laborious assembly operations.

4. Applications

Pressure-driven gas-diffusion/permeation micropumps have proved to be the most advantageous type of passive micropump owing to their perfect pumping performance under extreme conditions, *e.g.* a 3D-configurated microchannel at high temperature, several meter long microchannels, complex topological microsystems such as microvascular networks interconnecting multiple inlets and outlets and multi-phased microdroplet transport, as systematically demonstrated in this section.

4.1 Applications in extreme environments for velocity-stable liquid transport inside long microchannels at high temperature

In contrast with vacuum-driven gas-diffusion/permeation micropumps and most other passive micropumps, pressure-driven gas-diffusion/permeation micropumps can benefit from several inherent advantages.

Firstly, concerning the micro-processing that requires high reaction temperature like PCR, a denature temperature of 95 °C should be applied during the thermal cycling. Because such a high temperature is close to the boiling point of water, microbubbles can easily form after the aqueous solution is introduced into the microdevice if placed under atmospheric or vacuum conditions, which can totally destroy the flow stability.

Even though several self-powered micropumps have been developed, based on the aforementioned actuation mechanisms, few of them can stably deliver liquid inside long microchannels (*e.g.* several meters) at a high temperature (*e.g.* over 90 °C). Due to the serious vapour bubble problem, it is impossible to guaranteed satisfactory performance during a micro-continuous PCR concerning both passive micropumps and externally-powered micropumps. As a result, highly viscous media (*e.g.* mineral oil), pressurized microchannels or complicated bonding techniques should be applied to suppress the bubble formation inside the microchip at a high temperature.

As systematically demonstrated in our previous works, the formation or elimination of bubbles can be determined by the summation of three multi-directional forces (the force from the outer surroundings F_O, the gas expansion pressure F_I, and the surface tension of the liquid F_S) being exerted from the inner and outer surroundings of the air pockets.

If the following equation is fulfilled,

$$F_O + F_s > F_1$$

Then, bubble maturation can be suppressed. F_O is virtually the inner pressure of the liquid, which can be derived by combining the Navier–Stokes pressure[10] and air pressure inside the microchannel. Pressure-driven gas-diffusion/permeation micropumps rely on a much higher inner air-pressure than that of the outer atmosphere, and benefit from this, in that the microbubble formation inside the PDMS, glass, polymer and silicone microchannels under high temperature are efficiently suppressed.

In order to reveal their superiority, a self-powered pressure-driven gas-diffusion/permeation micropump was utilized for micro continuous PCR. The conditions of self-powered micro continuous PCR are more complicated than for most other chemical or biological processes inside microfluidic chips, which requires a strong micropump to overcome vapor bubbles at a high temperature (the 95 °C denature temperature), a several meters long PCR microchannel, which requires a powerful micropump with persistent motivating ability, and a homogeneous retention time for each amplification cycle, which requires a velocity-stable micropump. For example, it is impossible to inject a PCR sample into a PDMS-Glass microchannel just by syringe pump. As shown in Fig. 6B, a lot of air bubbles come out if the syringe pump is applied for ink transport. In contrast, the air bubbles can be eliminated if mineral oil is utilized to sandwich either the red ink (Fig. 6B-a–B-c) or the PCR sample (Fig. 6B-f).

However, if a pressure-driven gas-diffusion/permeation micropump is applied for sample transport through a PDMS-glass device, as shown in Fig. 6A, there are very few air bubbles that come out without the assistance of mineral oil. This verifies that the pressure-driven gas-diffusion/permeation micropump provides not only stable flow over a long distance, but also a steady flow that can endure high temperatures.

Secondly, the pressure-driven gas-diffusion/permeation micropump can be utilized with a wide range of chip-materials, not limited to PDMS. For a vacuum-driven gas-diffusion/permeation micropump, PDMS should be involved either for chip fabrication (especially for diffusion-type pumps) or the fabrication of a permeable membrane/wall.[97] For pressure-driven gas-diffusion/permeation micropumps, the sample can homogeneously flow inside a microchannel made from any type of gas-impermeable conduit (glass, plastic, metal, *etc.*), with the same actuation mechanism as a PMMA-PMMA microdevice. Thus, any gas-impermeable material can be used to fabricate the chip. As a result, this new self-activated micropump demonstrates potential for sample transport inside different microdevices without any power consumption.

Thirdly, self-powered pressure-driven gas-diffusion/permeation micropumps display superiority over self-powered vacuum-driven gas-diffusion/permeation micropumps in terms of both the pumping instantaneity and device compactness. For degassed micropumping, utilizing the gas solubility of PDMS, the PDMS devices need to be pre-vacuumed for a sufficient time and be stored in an air-tight package before use. Once the device is filled with liquid, the micropumping will no longer work, as previously demonstrated.[97] But, herein, for pressure-driven gas-diffusion/permeation micropumps, the micropumping can be reapplied to the same microchip even after being filled with liquid, and there is no need for the microchip to be pre-vacuumed/pressurized or stored in an air tight package. For micropumping utilizing the gas permeability of PDMS, either a PDMS membrane or a PDMS wall should be employed, which increase the fabrication cost and time (bonding and alignment are needed) and decrease the density of the microfluidic channel, since a lot of surrounding pneumatic microchambers also take up some space.[97] However, in contrast, there is neither an increase in the fabrication cost/time nor a decrease in the density of the microfluidic channels when applying pressure-driven gas-diffusion/permeation micropumps.

Although vacuum-driven gas-diffusion/permeation micropumps have been applied in point-of-care (POC) diagnosis, most of these applications were limited to simple conditions: a short microchannel under room temperature that does not require long-time pumping. In contrast, without external energy consumption or complicated constituent components, diffusion micropumps make the overall size much smaller than mechanical pumps, such as syringe pumps. Fig. 6D compares the sizes of the overall systems needed to operate the microdevice by self-powered pressure-driven gas-diffusion/permeation micropump (D-a) and syringe pump (D-b) to perform on-chip flow-through PCRs. The self-powered pressure-driven gas-diffusion/permeation micropump system requires neither tailor-made heating blocks nor expensive syringe pumps, but simply requires a hot plate and disposable plastic syringes for facile operation.

The successful application of pressure-driven gas-diffusion/permeation micropumps in PCR displays their advantages of enduring a high temperature, durable liquid driving strength and high flow stability. In contrast with the aforementioned micropumps, pressure-driven gas-diffusion/permeation micropumps have a lot of advantages, as they are much smaller in size, are free external energy driven, have simple fabricating procedures, strong micro fluidic transportation ability, have homogeneous flow velocity over a long distance, are resistant to adverse external conditions such as high temperature, have easy μTAS integration and are much lower in price.

4.2 Applications in a biomimetic microvasculature with multi-directional channels for bubble-free liquid injection

In most previous works[86,88–90] self-powered autonomous flow is applied to simple topological microsystems with a one-directional microchannel connecting of only one inlet and one outlet.

In contrast, leaf inspired microsystems consist of very complicated microvascular networks that interconnect multiple inlets and outlets, which is a totally different microstructural topology to that of the aforementioned microsystems. Noticeably, water transport in real leaves depends on self-activated micropumping without power consumption, similar to self-powered micropumps, as we introduced before. Inspired by this, biomimetic PDMS leaves were fabricated for visual assays of self-powered autonomous flow in real leaves.

As clarified in Fig. 7(A-a), "transpiration theory"[98,99] is the most widely accepted theory that explains self-powered water-pumping inside plants. Transpiration is the loss of water from a plant in the form of vapor. The idea behind this theory is that vapor molecules diffuse from inside the leaves to the outside atmosphere through the stomata, reducing hydrodynamic potential in the leaf and automating self-powered flow. In contrast, few stomata are located in the stipe, and thus, vapor molecule diffusion in the stipe is negligible, compared with that in a leaf. As a result, the hydrodynamic potential can be considered as a constant at the site of the stipe. Because vapor diffusion only reduces the hydrodynamic potential in the leaf and does not decrease the hydrodynamic potential in the stipe, a pressure gradient forms between the stipe and leaf, and pushes liquid autonomously from the stipe to the leaf after vapor-molecule diffusion. Similarly, air molecule diffusion only occurs in PDMS leaves and is negligible in the syringe.

Specialized to the self-powered flow inside the PDMS leaves, both the inlet tube and disposable syringe can be considered as gas-impermeable because the syringe material is made from PP and thus is impermeable to air molecules, but PDMS leaves are considered to be gas-permeable. As a result, gas permeability in the posterior part of the sample plug can be considered to be negligible, while air molecules can only diffuse from the two surfaces of the PDMS leaves to the atmo-

sphere. Due to the permeability of PDMS leaves, the pressurized air captured inside the biomimetic microvasculature diffuses through the artificial leaves, causing decreased pressure and continuous flow towards the biomimetic microvascular network from the syringe. The ideal gas law is as follows:

$$PV = nRT$$

where P is the pressure of the syringe, V is the volume, n is the number of air molecules inside the syringe, T is the temperature in Kelvin, and R is the gas constant.

Because the syringe is impermeable to air molecules, n can be reckoned to be a constant, from the above equation. Since the syringe volume is several hundred times that of the pipette combined with the microvascular network, the air volume V inside a gas-tight syringe can also be considered to be constant. Besides this, R and T are also constant in the above equation, so it can be concluded that P is also a constant. After the red ink flows through the inlet tube and reaches the biomimetic network of the PDMS leaves, the pressure of the posterior part can be maintained (by pushing the piston from the 4.3 mL mark to the 3.2 mL mark of the syringe) at 2.57 atm, but the pressure of the anterior part continues to decrease due to continuous air molecule diffusion. As a result, the red ink can finally fill the whole microvascular network of the PDMS leaves, as shown in Fig. 7B. From the above discussion, we can see that the air pressure throughout the entirety of the PDMS leaves is the same as before the sample plug flows into the inlet tube. After the sample is introduced into the inlet tube, the sample plug divides the fluidic conduit into two parts, wherein air molecules only permeate through the anterior part (PDMS leaves) but not at the posterior part (syringe), and thus, this results in a lower pressure at the anterior part than the posterior part. It can be reckoned that only the hydrodynamic potential of the PDMS leaves reduces, and that the hydrodynamic potential of the syringe does not decrease, similar to in a real leaf.

Based on the aforementioned discussion, it can be seen that even if self-powered flow through a real leaf and PDMS leaf differ in terms of the diffusion of gas molecules (air molecule diffusion in a PDMS leaf, but vapor molecule diffusion in a real leaf), they share the same gas molecule diffusion mediated pumping mechanism for the same microvascular geometry (from inside the PDMS/real leaf into the atmosphere). Mostly important, the liquid flux in both cases can be represented by the following equation:

$$Q = V_{\mathrm{d}}$$

where Q is the liquid flux, while V_{d} is the diffusion volume (per minute) of the vapor molecule or gas molecule through the real leaf or PDMS leaf.

As a result, a gas diffusion mediated overall hydraulic pressure gradient is imposed on the same microvascular geometry in both PDMS leaves and real leaves, which causes a similar hydrodynamic flux through microvascular networks. So, nature-inspired PDMS leaves, as introduced here, can act as a lab-on-a-chip platform for hydrodynamic flux analysis, in the manner of a veinal microvasculature of a natural leaf, as an alternative to conventional approaches.

As also shown in Fig. 7B, after the fluid totally fills the whole microvascular network, lots of air bubbles are distributed on the underside of the PDMS leaf, confirming that air molecules diffuse from pressurized PDMS leaves into the ambient atmosphere during autonomous flow.

4.3 Applications in multi-phased microfluidics for autonomous microdroplet generation/transport

It is still a key challenge to apply traditional passive micropumps for stable and autonomous generation/transport of microdroplets. In contrast with traditional passive micropumps, it has been found that pressure-driven gas-diffusion/permeation micropumps can maintain the stable generation/transport of microdroplets inside a fluidic conduit. As shown in Fig. 8, only two disposable syringes are required to autonomously generate and transport microdroplets inside a 3D microchannel of several meters in length. The proposed mechanism also depends on air permeation from the compressed microchip to the ambient environment through a gas-permeable tube. However, the main difference compared with previous systems is that, the continuous and dispersed phases

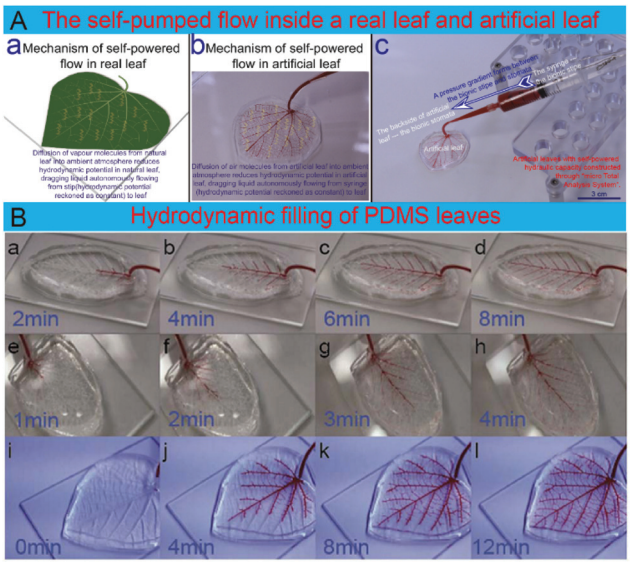

Fig. 7 (A) The mechanism of self-pumped flow inside a real leaf and an artificial leaf. (A-a) A schematic of a self-pumped flowing mechanism in a real leaf. The brown arrows under the schematic leaf represent the diffusion and evaporation of vapor molecules from the leaf into the atmosphere. (A-b) The self-pumped flowing mechanism in the artificial leaf. The brown arrows under the PDMS leaf represent the diffusion and evaporation of air molecules from the leaf into the atmosphere. (A-c) The filling of the microvascular network of PDMS replicates using only an inlet channel. (B) Hydrodynamic filling of PDMS leaves: (B-a)–(B-d) Carpinus betulus, (B-e)–(B-h) Aegopodium podagraia, and (B-i)–(B-l) Tilia platyphyllos, images were obtained at 2, 1, and 4 min intervals, respectively. Reproduced from ref. 87 with permission from the Royal Society of Chemistry, copyright 2016.

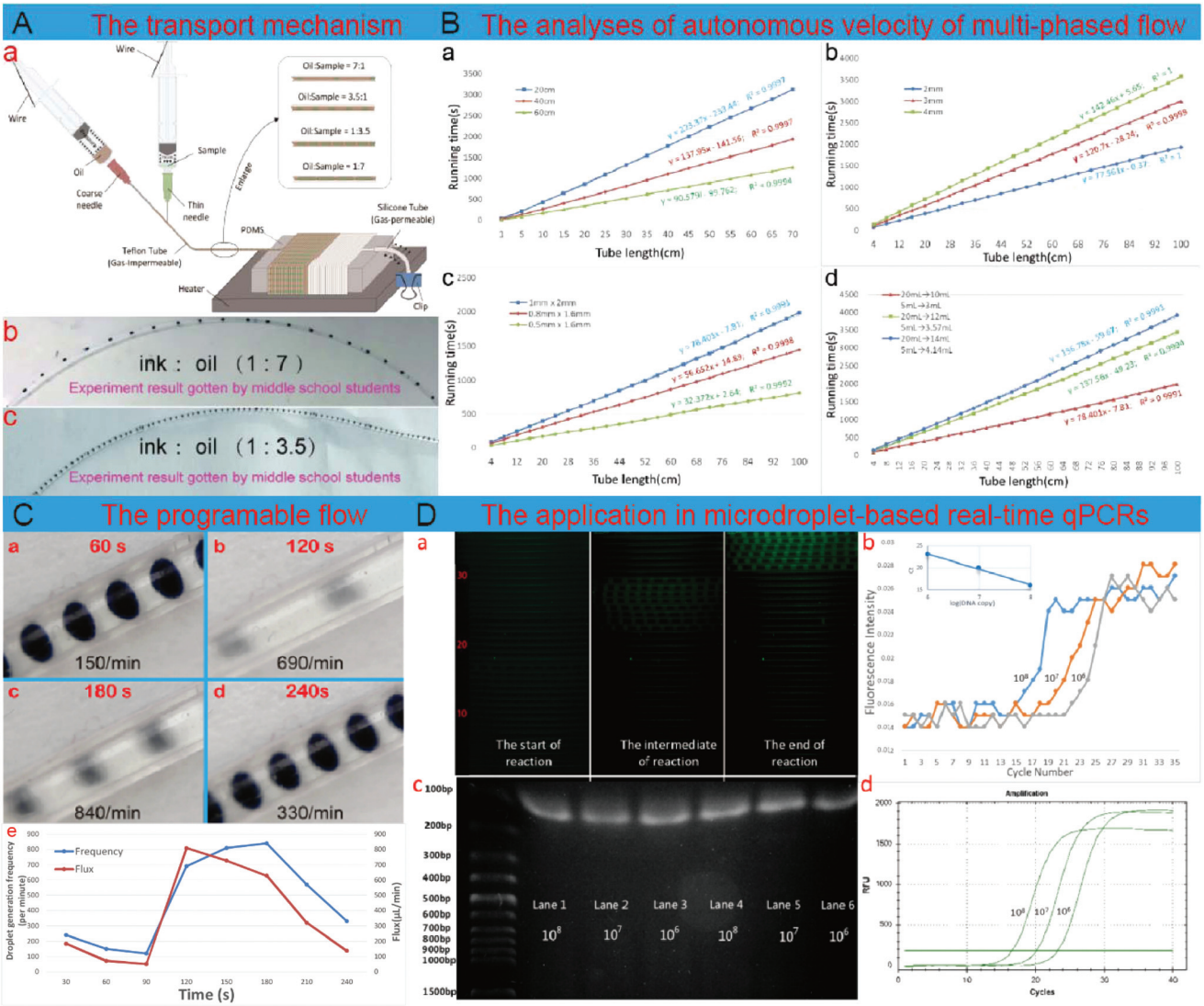

Fig. 8 Applications of a pressure-driven gas-diffusion/permeation micropump for multi-phase microfluidic transport. (A) Autonomous microdroplet generation inside the microdevice. (A-a) A schematic of the set-up of the experiment. (A-b) The experimental result (ink : oil = 1 : 7) obtained by middle school students. (A-c) The experimental result (ink : oil = 1 : 3.5) obtained by middle school students. (B) Quantitative analyses of the proposed self-activated droplet generation inside Teflon tubes (I.D. 1 mm, O.D. 2 mm). (B-a) The effect of the lengths of outlet silicone tubes on the flow rate and total running time, when the outer diameter and inner diameter of the outlet silicone tubes were 3 and 1.5 mm, respectively. (B-b) Results of the total running time inside a 100 cm long Teflon tube by varying the outer diameter of the outlet silicone tube. (B-c) A graph showing the flow rate change for different inner diameters of the Teflon microchannel, when the same length of microchannel and outlet silicone tube were used. (B-d) Comparison of the total running time by varying the initial internal pressure. The linear-regression analysis and R^2 value of each of the flow conditions were calculated and are displayed near the curves. (C) The programmable controllability of the pressure-driven gas-diffusion/permeation micropump for application in the autonomous control of multi-phase microfluidics, with the numbers of droplets generated per minute programmed to be 150, 690, 840, and 330, for running times of 60, 120, 180, and 240 s, respectively. Correspondingly, the fluidic flux of the aqueous phase decreased from 190 to 50 μL min^{-1} between 30 and 90 s, and then increased to 810 μL min^{-1} at 120 s, before finally decreasing to 130 μL min^{-1} at 240 s. (D) Real time qPCR results. (D-a) Series of images showing the droplet reaction to DNA amplification inside the 3D spiral Teflon microchannel. (D-b) Serial dilution of the PCR amplification curves from the fluorescence images inside the 3D spiral Teflon microchannel. (D-c) Results of the DNA amplification inside the Teflon tube or real-time PCR amplification system (Bio-Rad CFX96). Lanes 1, 2 and 3 show the target amplicons obtained using a spiral Teflon microchannel, lanes 4, 5 and 6 show the target amplicons obtained using a commercial PCR amplification system. (D-d) Amplification curves from the commercial real-time PCR amplification system. Reproduced from ref. 100 with permission from the Royal Society of Chemistry, copyright 2018.

are loaded together into the inlet of the microdevice. Because of this, the aqueous-phase and oil-phase are actuated parallelly to the microchip, with homogeneous microdroplets generated at the junction. The aqueous droplet volume fraction can be controlled by the volume ratio of compressed air between the two syringes, resulting in size-controllability during transport.

Most importantly, the set-up of the pumping system is also very simple, requiring only a microfluidic tube and a few hand-

operated syringes without the need for any sophisticated fabrication, bonding or microchannel-surface modification procedures, making the entire system user-friendly and accessible to non-technical users. For instance, after just 2 hours of training, middle school students without professional skills, who previously knew nothing about microfluidics previously, were able to easily grasp the use of a pressure driven gas-diffusion/permeation micropump for applications in autonomous microdroplet generation and long distance transport, for volume ratios between the ink droplet and oil intervals varying from 1 : 7 to 1 : 3.5, respectively (Fig. 8A). So, the pressure-driven gas-diffusion/permeation micropump is a potential tool for teaching microfluidics knowledge in education laboratories, or multiphase microfluidic applications in ordinary chemistry/biology labs with limited resources. As shown in Fig. 8A, when the volume ratios of compressed air between the oil-phase syringe and aqueous-phase syringe were 7 : 1, 3.5 : 1, 1 : 1 and 1 : 7, a similar aqueous droplet volume fraction was confirmed.

Another big advantage of pressure-driven gas-diffusion/permeation micropumps is that, the long-distance autonomous flow rate inside a 3D microchannel is highly stable, with an average R^2 value calculated as 0.9995 after linear regression analysis during the microdroplet transport, which is much more stable than for other types of self-activated micropumps (Fig. 8B). In addition, both the generation frequency and transport rate of microdroplets can be easily programmed by adjusting a vent valve connected to the outlet of the microchannel (Fig. 8C).

For most micropumps, surfactants are required to be added to either the continuous phase or the dispersed phase, or both to avoid fusion when transporting microdroplets. Amazingly, when a pressure-driven gas-diffusion/permeation micropump is applied in the autonomous control of multi-phased microfluidics inside a PTFE tube-based fluidic conduit, no surfactant is required, and fusion-free droplets can be transported at a high temperature.

As a proof of concept, this micropump was applied for microdroplet transport inside a 3D spiral microchip for flow-through on-chip real-time PCRs. Without adding any surfactant, no droplet-fusion was detected during the thermo cycle when the microdroplet flew up and down the 3D microchannel of several meters in length. Based on 3 ordered serially diluted reference genes used in both the commercial qPCR cycler (Bio Rad) and the home-made microdevice, similar amplification results were observed between the two systems, with calculated C_t values of 15.92, 20.07 and 23.22 for the microdevice, and 16.51, 20.1, and 23.15, for the commercial cycler. The overall amplification efficiency of the microdevice was almost the same as that of the commercial cycler from gel analysis, verifying that the pressure-driven gas-diffusion/permeation micropump is acceptable for droplet-based continuous flow microfluidic PCRs with comparable thermocycle control and real-time fluorescence signal as a commercial cycler (Fig. 8D).

4.4 Outlook

In previous works, pressure-driven gas-diffusion/permeation micropumps have been successfully applied in extreme microenvironments, such as three-dimensional, long-distance droplet/plug transport in a multi-directional microchannel at high temperatures, which proves that it is a powerful micropump format.

To be improved as a mature micropumping technique, the programing capability and on/off valving control should also be clarified. Recently, smart flow has been proposed using various self-powered pumping methods from different automation approaches. For instance, the use of light has been confirmed as an effective way to realize remote pumping control for surface tension-driven micropumps[101,102] and self-automated chemical micropumps.[103] The heat effect caused by light explosion[101] or electricity can also play the role of a valving function for capillary flow. Mechanical motion can be reckoned as another potential approach to turn on/off self-powered flow activated by surface tension-driven micropumps[104] and vacuum-driven gas-diffusion/permeation micropumps. Because little research has been done on applying pressure-driven gas-diffusion/permeation micropumps for smart on/off flow control by external signals, it may become an interesting field in the near future.

5. Conclusions

In brief summary, technological developments during the last ten years have made it quite cheap, easy and quick to fabricate microdevices. As a result, the concept of disposable microchips for clinical detection, biological analysis, and disease diagnosis, *etc.*, has become possible and is becoming increasingly valued. However, most disposable microdevices still rely on other accessories to finally realize functionalization. Necessary accessories always include micropumps, microheaters, microvalves and micromixers, *etc.* Only in the case of when a disposable microdevice matches well with its accessories can the disposable microdevice realize its value and significance. From this angle, not only should the easily fabricated microdevice be cheap or disposable, its accessories (*i.e.* various types of micropumps, such as electroosmotic micropumps, magnetohydrodynamic micropumps, electrokinetic micropumps, electrophoresis micropumps, *etc.*) should also be easily fabricated, cheap, portable and even disposable. And thus, in contrast with externally-powered micropumps, self-powered micropumps can definitely play more of an important role in liquid transport inside self-contained microdevices.

However, to precisely modulate the flow rate on the micro scale is a challenge for most traditional self-powered micropumps. The use of pressure-driven gas-diffusion/permeation micropumps is a promising way to realize precise spatial and temporal control over the flow rate. Because of their unique superiority of integrating so many advantages, pressure-driven gas-diffusion/permeation micropumps are different from traditional self/external powered micropumps, as systemically discussed in this review. Through detailed flow analyses inside different microdevices, it has been verified that pressure-driven gas-diffusion/permeation micropumps not only provide

stable flow over a long distance, but can also easily (just by changing the microdevice dimensions and operating parameters) modulate a much wider range of flow rates than traditional self-powered micropumps (*e.g.* surface tension-driven micropumps, hydrostatic pressure-driven micropumps, vacuum-driven gas-diffusion/permeation micropumps, and chemical/enzymatic/biological micropumps). When we apply pressure-driven gas-diffusion/permeation micropumps to micro continuous PCR inside a microchip, it can be verified that pressure-driven gas-diffusion/permeation micropumps can automate the stable flow of microdroplets/plug through a 3D channel over several meters in length, and perfectly suppress the vapor/boiling bubbles that form at a high denaturing temperature of 95 degrees. Unlike other self-powered micropumps, which are generally limited to hydrophilic (surface tension-driven micropumps) or gas-permeable microchannels (vacuum-driven gas-diffusion/permeation micropumps), pressure-driven gas-diffusion/permeation micropumps can be applied to liquid transport inside microchannels made from any type of material (*e.g.* PMMA, PTFE, FEP, PDMS, PVC, silicone, PC, glass, PET, *etc.*). We also made a comparison between pressure-driven gas-diffusion/permeation micropumps and external-powered micropumps in terms of their performance, which also revealed that pressure-driven gas-diffusion/permeation micropumps perform better at a high temperature. When using a syringe pump, a lot of bubbles come out from the microchannel, which even totally break the liquid flow. However, when using a diffusion micropump, few bubbles come out from the device. Because the flow is so stable, without any microbubble formation, the PCR amplification is highly efficient here.

No doubt this new micropump will have great significance in lots of different fields, such as the biomedical field and life sciences – not only in only in terms of basic research, but also in terms of its commercial prospect, on account of its simple structure, ease of fabrication, compact size, high precision, low power consumption, and relatively fast response time. Nevertheless, there have not been any traditional micropumps that have been capable of realizing all of these advantages together, reflecting the great prospects of pressure-driven gas-diffusion/permeation micropumps. We hope that microfluidics and μTAS communities can harness gas-diffusion/permeation mechanisms to develop various types of self-contained pumping microdevices to solve biological, chemical, medical and other challenges.

Conflicts of interest

There are no conflicts of interest to declare.

Acknowledgements

This project was supported by the CAS Pioneer Hundred Talents Program, the National Natural Science Foundation of China (No. 61704169), the Natural Science Foundation of Jilin Province (20180520112JH), and the talent project of Jilin Province.

References

1 H. Van lintel, F. Van depol and S. Bouwstra, *Sens. Actuators*, 1988, **15**, 153–167.
2 J. G. Smits, *Sens. Actuators, A*, 1990, **21**, 203–206.
3 D. J. Laser and J. G. Santiago, *J. Micromech. Microeng.*, 2004, **14**, R35–R64.
4 P. Woias, *Sens. Actuators, B*, 2005, **105**, 28–38.
5 S. Yokota, *Mech. Eng. Rev.*, 2014, **1**, M14.
6 M. Nabavi, *Microfluid. Nanofluid.*, 2009, **7**, 599–619.
7 A. K. Au, H. Lai, B. R. Utela and A. Folch, *Micromachines*, 2011, **2**, 179–220.
8 C. Zhang, D. Xing and Y. Li, *Biotechnol. Adv.*, 2007, **25**, 483–514.
9 K. T. L. Trinh, W. Wu and N. Y. Lee, *Sens. Actuators, B*, 2014, **190**, 177–184.
10 W. Wu, K. Kang and N. Y. Lee, *Analyst*, 2011, **136**, 2287.
11 W. Wu, T. L. T. Kieu and N. Y. Lee, *Analyst*, 2012, **137**, 2069–2076.
12 W. Wu and N. Y. Lee, *Anal. Bioanal. Chem.*, 2011, **400**, 2053–2060.
13 W. Wu, J. Wu, J. Kim and N. Y. Lee, *Lab Chip*, 2015, **15**, 2819–2825.
14 M. A. Rezaienia, G. Paul, E. Avital, A. Rahideh, M. T. Rothman and T. Korakianitis, *J. Biomech.*, 2016, **49**, 1865–1872.
15 S. B. Shim, Y. J. Park, J. M. Kim and K. U. Kim, *J. Mech. Sci. Technol.*, 2015, **29**, 759–767.
16 U. Sönmez, M. Bekin and L. Trabzon, MATEC Web of Conferences, 2018, vol. **153**, p. 8002.
17 T. N. Gerasimenko, O. V. Kindeeva, V. A. Petrov, A. I. Khaustov and E. V. Trushkin, *Applied Mathematical Modelling*, 2017, **52**, 590–602.
18 T. Leu, D. Gong and D. Pan, *Microsyst. Technol.*, 2017, **23**, 329–341.
19 A. M. Nightingale, G. W. H. Evans, P. Xu, B. J. Kim, S. Hassan and X. Niu, *Lab Chip*, 2017, **17**, 1149–1157.
20 V. Saller, J. Matilainen, U. Grauschopf, K. Bechtold-Peters, H. Mahler and W. Friess, *J. Pharm. Sci.*, 2015, **104**, 1440–1450.
21 Y. J. Ren, Y. T. Ma, D. Huang, J. Chen and Z. H. Feng, *Sens. Actuators, A*, 2016, **244**, 126–132.
22 S. C. Lee, S. Hur, D. Kang, B. H. Kim and S. J. Lee, *Bioinspiration Biomimetics*, 2016, **11**(3), 036006.
23 H. Feth, F. Pothof, F. Thoma, T. Schmidt, C. Mueller, F. Goldschmidtboeing and P. Woias, *Microsyst. Technol.*, 2014, **20**, 1299–1310.
24 Z. Chen, P. Liao, F. Zhang, M. Jiang, Y. Zhu and Y. Huang, *Lab Chip*, 2017, **17**, 235–240.

25 J. Ni, B. Li and J. Yang, *Microelectron. Eng.*, 2012, **99**, 28–32.
26 J. S. Paustian, A. J. Pascall, N. M. Wilson and T. M. Squires, *Lab Chip*, 2014, **14**, 3300–3312.
27 N. Islam and J. Reyna, *Electrophoresis*, 2012, **33**, 1191–1197.
28 J. M. Karlinsey, *Anal. Chim. Acta*, 2012, **725**, 1–13.
29 Q. Yuan and J. Wu, *Biomed. Microdevices*, 2013, **15**, 125–133.
30 D. Tripathi, R. Jhorar, O. Anwar Bég and A. Kadir, *J. Mol. Liq.*, 2017, **236**, 358–367.
31 M. Rivero and S. Cuevas, *Sens. Actuators, B*, 2012, **166**, 884–892.
32 H. Kumamaru, *Int. J. Mech. Eng. Appl.*, 2017, **5**, 247.
33 R. Yang, H. Hou, Y. Wang and L. Fu, *Sens. Actuators, B*, 2016, **224**, 1–15.
34 C. N. Kim, *Comput. Fluids.*, 2014, **104**, 30–39.
35 J. Ni, B. Wang, S. Chang and Q. Lin, *Microelectron. Eng.*, 2014, **117**, 35–40.
36 S. Sugimoto, M. Hara, H. Oguchi and H. Kuwano, *J. Microelectromech. Syst.*, 2015, **24**, 696–702.
37 F. G. Strobl, D. Breyer, P. Link, A. A. Torrano, C. Braeuchle, M. F. Schneider and A. Wixforth, *Beilstein J. Nanotechnol.*, 2015, **6**, 414–419.
38 S. Chakraborty, *Lab Chip*, 2005, **5**, 421–430.
39 G. Munchow, D. Dadic, F. Doffing, S. Hardt and K. S. Drese, *Expert Rev. Mol. Diagn.*, 2005, **5**, 613–620.
40 H. Ren, S. Xu and S. Wu, *Lab Chip*, 2013, **13**, 100–105.
41 P. Kauffman, E. Fu, B. Lutz and P. Yager, *Lab Chip*, 2010, **10**, 2614–2617.
42 P. Chen, Y. Cheng, K. Young, H. Hsieh and C. Yang, *Int. J. Precis. Eng. Man.*, 2016, **17**, 1547–1554.
43 H. Jeong, S. Lee and C. Lee, *Biosens. Bioelectron.*, 2013, **47**, 278–284.
44 N. Ramalingam, M. E. Warkiani, N. Ramalingam, G. Keshavarzi, H. Liu and T. G. Hai-Qing, *Biomed. Microdevices*, 2016, **18**(4), 68.
45 T. Zhang and T. Cui, *IEEE*, 2011, pp. 606–609.
46 R. Safavieh, A. Tamayol and D. Juncker, *Microfluid. Nanofluid.*, 2015, **18**, 357–366.
47 L. Gervais, M. Hitzbleck and E. Delamarche, *Biosens. Bioelectron.*, 2011, **27**, 64–70.
48 F. R. de Souza, G. L. Alves and W. K. Tomazelli Coltro, *Anal. Chem.*, 2012, **84**, 9002–9007.
49 B. Eker, Y. Temiz and E. Delamarche, *Biomed. Microdevices*, 2014, **16**, 829–835.
50 K. L. Dornelas, N. Dossi and E. Piccin, *Anal. Chim. Acta*, 2015, **858**, 82–90.
51 R. Safavieh and D. Juncker, *Lab Chip*, 2013, **13**, 4180–4189.
52 M. Jang, C. K. Park and N. Y. Lee, *Sens. Actuators, B*, 2014, **193**, 599–607.
53 W. Wu and A. Manz, *RSC Adv.*, 2015, **5**, 70737–70742.
54 E. Holczer and P. Fuerjes, in *Procedia Engineering*, ed. G. Sberveglieri and V. Ferrari, 2014, vol. 87, pp. 492–495.
55 S. Huang, J. Song, Y. Lu, C. Lv, H. Zheng, X. Liu, Z. Jin, D. Zhao, C. J. Carmalt and I. P. Parkin, *J. Mater. Chem. A*, 2016, **4**, 13771–13777.
56 T. Kokalj, Y. Park, M. Vencelj, M. Jenko and L. P. Lee, *Lab Chip*, 2014, **14**, 4329–4333.
57 X. Wang, J. A. Hagen and I. Papautsky, *Biomicrofluidics*, 2013, **7**, 014107.
58 M. I. Mohammed and M. P. Y. Desmulliez, *Microsyst. Technol.*, 2013, **19**, 809–818.
59 M. Marimuthu and S. Kim, *Anal. Biochem.*, 2013, **437**, 161–163.
60 A. Maki, S. Hemmila, J. Hirvonen, N. N. Girish, J. Kreutzer, J. Hyttinen and P. Kallio, *J. Fluids Eng.*, 2015, **137**, 0211052.
61 I. You, S. M. Kang, S. Lee, Y. O. Cho, J. B. Kim, S. B. Lee, Y. S. Nam and H. Lee, *Angew. Chem., Int. Ed.*, 2012, **51**, 6126–6130.
62 Z. Li, Y. Zhao, D. Zhang, S. Zhuang and Y. Yamaguchi, *Sens. Actuators, B*, 2016, **230**, 779–784.
63 I. K. Dimov, L. Basabe-Desmonts, J. L. Garcia-Cordero, B. M. Ross, Y. Park, A. J. Ricco and L. P. Lee, *Lab Chip*, 2011, **11**, 4279.
64 K. Hosokawa, K. Sato, N. Ichikawa and M. Maeda, *Lab Chip*, 2004, **4**, 181.
65 J. Li, Y. Huang, D. Wang, B. Song, Z. Li, S. Song, L. Wang, B. Jiang, X. Zhao, J. Yan, R. Liu, D. He and C. Fan, *Chem. Commun.*, 2013, **49**, 3125–3127.
66 Y. Shin, J. Z. Barnett, E. Song, M. T. Gutierrez-Wing, K. A. Rusch and J. Choi, *Microelectron. Eng.*, 2015, **144**, 6–11.
67 J. T. Nevill, A. Mo, B. J. Cord, T. D. Palmer, M. Poo, L. P. Lee and S. C. Heilshorn, *Soft Matter*, 2011, **7**, 343–347.
68 D. Y. Liang, A. M. Tentori, I. K. Dimov and L. P. Lee, *Biomicrofluidics*, 2011, **5**(2), 024108.
69 Q. Zhu, L. Qiu, B. Yu, Y. Xu, Y. Gao, T. Pan, Q. Tian, Q. Song, W. Jin, Q. Jin and Y. Mu, *Lab Chip*, 2014, **14**, 1176–1185.
70 T. Tang, G. Li, C. Jia, K. Gao and J. Zhao, *Biomicrofluidics*, 2014, **8**, 026501.
71 C. Li, J. Xu and B. Ma, *Microfluid. Nanofluid.*, 2015, **18**, 1067–1073.
72 R. M. Feeny, N. L. Puissant and C. S. Henry, *Anal. Methods*, 2016, **8**, 8266–8271.
73 L. Xu, H. Lee and K. W. Oh, *Microfluid. Nanofluid.*, 2014, **17**, 745–750.
74 M. A. Eddings and B. K. Gale, *J. Micromech. Microeng.*, 2006, **16**, 2396–2402.
75 Q. Tian, Q. Song, Y. Xu, Q. Zhu, B. Yu, W. Jin, Q. Jin and Y. Mu, *Anal. Methods*, 2015, **7**, 2006–2011.
76 M. Kolnik, L. S. Tsimring and J. Hasty, *Lab Chip*, 2012, **12**, 4732–4737.
77 A. R. Abate and D. A. Weitz, *Biomicrofluidics*, 2011, **5**, 14107.
78 C. Zhou, H. Zhang, Z. Li and W. Wang, *Lab Chip*, 2016, **16**, 1797–1811.

79 H. Zhang, W. Duan, M. Lu, X. Zhao, S. Shklyaev, L. Liu, T. J. Huang and A. Sen, *ACS Nano*, 2014, **8**, 8537–8542.
80 S. Sengupta, D. Patra, I. Ortiz-Rivera, A. Agrawal, S. Shklyaev, K. K. Dey, U. Cordova-Figueroa, T. E. Mallouk and A. Sen, *Nat. Chem.*, 2014, **6**, 415–422.
81 D. Patra, H. Zhang, S. Sengupta and A. Sen, *ACS Nano*, 2013, **7**, 7674–7679.
82 J. J. McDermott, A. Kar, M. Daher, S. Klara, G. Wang, A. Sen and D. Velegol, *Langmuir*, 2012, **28**, 15491–15497.
83 Y. Tanaka, Y. Noguchi, Y. Yalikun and N. Kamamichi, *Sens. Actuators, B*, 2017, **242**, 1186–1192.
84 D. Patra, S. Sengupta, W. Duan, H. Zhang, R. Pavlick and A. Sen, *Nanoscale*, 2013, **5**, 1273–1283.
85 X. Noblin, L. Mahadevan, I. A. Coomaraswamy, D. A. Weitz, N. M. Holbrook and M. A. Zwieniecki, *Proc. Natl. Acad. Sci. U. S. A.*, 2008, **105**, 9140–9144.
86 W. Wu, K. T. L. Trinh and N. Y. Lee, *Analyst*, 2012, **137**, 983–990.
87 W. Wu, R. M. Guijt, Y. E. Silina, M. Koch and A. Manz, *RSC Adv.*, 2016, **6**, 22469–22475.
88 W. Wu, K. T. L. Trinha and N. Y. Lee, *Analyst*, 2015, **140**, 1416–1420.
89 W. Wu, K. T. L. Trinh, Y. Zhanga and N. Y. Lee, *RSC Adv.*, 2015, **5**, 12071–12077.
90 W. Wu and N. Y. Lee, *Sens. Actuators, B*, 2013, **181**, 756–765.
91 T. L. T. Kieu, W. Wu and N. Y. Lee, *RSC Adv.*, 2017, **7**, 10624–10630.
92 G. M. Whitesides, *Nature*, 2006, **442**, 368–373.
93 A. Boehm, F. Carstens, C. Trieb, S. Schabel and M. Biesalski, *Microfluid. Nanofluid.*, 2014, **16**, 789–799.
94 E. Elizalde, R. Urteaga and C. L. A. Berli, *Lab Chip*, 2015, **15**, 2173–2180.
95 A. Mäki, H. Samu, J. Hirvonen and P. Kallio, *J. Fluids Eng.*, 2014, 14–1238.
96 X. Y. Zhu, L. Y. Chu, B. H. Chueh, M. W. Shen, B. Hazarika, N. Phadke and S. Takayama, *Analyst*, 2004, **129**, 1026–1031.
97 L. Xu, H. Lee, D. Jetta and K. W. Oh, *Lab Chip*, 2015, **15**, 3962–3979.
98 T. D. Wheeler and A. D. Stroock, *Nature*, 2008, **455**, 208–212.
99 M. J. Canny, *Am. Sci.*, 1998, **86**, 152–159.
100 Y. Jiang, L. Du, Y. Liu, Q. Mu, Z. Cui, J. Zhou and W. Wu, *Analyst*, 2018, **143**, 3798–3807.
101 C. Huang, J. Lv, X. Tian, Y. Wang, J. Liu and Y. Yu, *Smart Mater. Struct.*, 2016, **25**(9), 095009.
102 J. Lv, Y. Liu, J. Wei, E. Chen, L. Qin and Y. Yu, *Nature*, 2016, **537**, 179.
103 V. Yadav, H. Zhang, R. Pavlick and A. Sen, *J. Am. Chem. Soc.*, 2012, **134**, 15688–15691.
104 M. Hitzbleck, L. Avrain, V. Smekens, R. D. Lovchik, P. Mertens and E. Delamarche, *Lab Chip*, 2012, **12**, 1972–1978.